Plant Physiology and Biochemistry 65 (2013) 17–26

Contents lists available at SciVerse ScienceDirect

Plant Physiology and Biochemistry

journal homepage: www.elsevier.com/locate/plaphy

Research article

Virus-induced gene silencing of pea *CHLI* and *CHLD* affects tetrapyrrole biosynthesis, chloroplast development and the primary metabolic network

Tao Luo [a,b,1], Sha Luo [e], Wagner L. Araújo [c,d], Hagen Schlicke [b], Maxi Rothbart [b], Jing Yu [a], Tingting Fan [a], Alisdair R. Fernie [c], Bernhard Grimm [b,**], Meizhong Luo [a,*]

[a] National Key Laboratory of Crop Genetic Improvement, Huazhong Agricultural University, Wuhan 430070, PR China
[b] Institute of Biology/Plant Physiology, Humboldt University, Philippstr. 13, Building 12, D 10115 Berlin, Germany
[c] Max-Planck-Institute of Molecular Plant Physiology, 14476 Potsdam-Golm, Germany
[d] Departamento de Biologia Vegetal, Universidade Federal de Viçosa, 36570-000 Viçosa, Minas Gerais, Brazil
[e] Department of Horticulture, College of Agronomy, Jiangxi Agricultural University, Nanchang 330045, PR China

ARTICLE INFO

Article history:
Received 14 December 2012
Accepted 4 January 2013
Available online 28 January 2013

Keywords:
Metabolite profiling
Mg chelatase subunit CHLD
Mg chelatase subunit CHLI
Pisum sativum
Tetrapyrrole biosynthesis
Virus-induced gene silencing

ABSTRACT

The first committed and highly regulated step of chlorophyll biosynthesis is the insertion of Mg^{2+} into protoporphyrin IX, which is catalyzed by Mg chelatase that consists of CHLH, CHLD and CHLI subunits. In this study, *CHLI* and *CHLD* genes were suppressed by virus-induced gene silencing (VIGS-*CHLI* and VIGS-*CHLD*) in pea (*Pisum sativum*), respectively. VIGS-*CHLI* and VIGS-*CHLD* plants both showed yellow leaf phenotypes with the reduced Mg chelatase activity and the inactivated synthesis of 5-aminolevulinic acid. The lower chlorophyll accumulation correlated with undeveloped thylakoid membranes, altered chloroplast nucleoid structure, malformed antenna complexes and compromised photosynthesis capacity in the yellow leaf tissues of the VIGS-*CHLI* and VIGS-*CHLD* plants. Non-enzymatic antioxidant contents and the activities of antioxidant enzymes were altered in response to enhanced accumulation of reactive oxygen species (ROS) in the chlorophyll deficient leaves of VIGS-*CHLI* and VIGS-*CHLD* plants. Furthermore, the results of metabolite profiling indicate a tight correlation between primary metabolic pathways and Mg chelatase activity. We also found that *CHLD* induces a feedback-regulated change of the transcription of photosynthesis-associated nuclear genes. *CHLD* and *CHLI* silencing resulted in a rapid reduction of photosynthetic proteins. Taken together, Mg chelatase is not only a key regulator of tetrapyrrole biosynthesis but its activity also correlates with ROS homeostasis, primary interorganellar metabolism and retrograde signaling in plant cells.

1. Introduction

The chlorophyll-synthesizing branch (Mg branch) of the tetrapyrrole pathway is initiated by the ATP-dependent insertion of Mg^{2+} into protoporphyrin IX, which is catalyzed by Mg chelatase. This first committed step in chlorophyll biosynthesis is highly regulated at the transcriptional and post-translational levels [1]. *In vitro* reconstitution studies of Mg chelatase complex using the subunits of *Rhodobacter sphaeroides* [2,3] and cyanobacterium *Synechocystis PCC6803* [4] as well as the analyses of yellow and pale green mutants of higher plants and green algae [5,6] have demonstrated that Mg chelatase is composed of three subunits (bacteria/eukaryotic subunit): BchH/CHLH, BchD/CHLD and BchI/CHLI. The catalytic mechanism of Mg chelatase includes at least two steps: an enzyme-activation step followed by a Mg^{2+} insertion step [7]. The activation step requires ATP, Mg^{2+} and the two subunits CHLI and CHLD to form the ring structure of the CHLI–CHLD–Mg–ATP complex [8]. These quaternary complex forms a platform for the protoporphyrin IX-binding CHLH subunit to insert Mg^{2+} into protoporphyrin IX under consumption of ATP in the insertion step [8,9]. Recently, GENOMES UNCOUPLED 4 (GUN4) has been identified as

Abbreviations: ALA, 5-aminiolevulinic acid; CHLD, CHLH and CHLI, Mg chelatase CHLD, CHLH and CHLI subunit; DAB, 3,3′-diaminobenzidine; DAPI, 4′,6-diamidino-2-phenylindole; GC–MS, gas-chromatography mass-spectrometry; *gun*, *genomes uncoupled*; NBT, nitroblue tetrazolium; PEBV, pea-early-browning-virus; PhANGs, photosynthesis-associated nuclear genes; ROS, reactive oxygen species; VIGS, virus induced gene silencing; VIGS-*CHLD*, virus-induced *CHLD* gene silencing; VIGS-*CHLI*, virus-induced *CHLI* genes silencing.

* Corresponding author. Tel./fax: +86 27 87284213.
** Corresponding author. Tel./fax: +49 30 20936119.
E-mail addresses: bernhard.grimm@rz.hu-berlin.de (B. Grimm), mzluo@mail.hzau.edu.cn (M. Luo).
[1] Present address: Center for Neuropsychiatric Diseases, Institute of Life Science, Nanchang University, Nanchang 330031, PR China.

0981-9428/$ – see front matter © 2013 Elsevier Masson SAS. All rights reserved.
http://dx.doi.org/10.1016/j.plaphy.2013.01.006

a CHLH-interacting and a protoporphyrin IX and Mg protoporphyrin IX-binding protein. It acts as a positive regulator that controls the flow of substrate into the chlorophyll branch [10]. Moreover, our recent studies have revealed that the C-terminal residues of GUN4 are required for activation of the CHLH subunit [11].

Alignment of the BchD/CHLD and BchI/CHLI amino acid sequences revealed a high degree of similarity between BchI/CHLI and the N-terminus of BchD/CHLD. Both subunits are classified as members of the AAA^{+} protein family, an extended class of the AAA family (ATPase associated with various cellular activities) [9]. CHLI functions as an ATPase, but CHLD fails to hydrolyze ATP [12]. The ATPase activity of CHLI is essential for Mg chelatase activity and is redox-regulated through the activity of thioredoxins [13,14]. Moreover, the ATPase activity of the CHLI subunit contributes to the stability of the CHLI/CHLD oligomer *in vivo* [15]. It stands to reason that the structural and functional link between CHLI and CHLD implies a vital regulatory role in the modulation of Mg chelatase activity *in vivo*.

In plants, the coordination of gene expression between nuclear and organellar genomes is essential for plant survival and adaption to environmental variations [16]. Thereby, through anterograde signaling, the nucleus-encoded protein factors control the expression of plastid-encoded genes and plastid-located proteins, while retrograde signaling integrate various forms of information from chloroplasts to the nucleus [16]. Arabidopsis *gun* (*genomes uncoupled*) mutants have been characterized to show modified retrograde signaling [17]. Among the five *gun* mutants reported (*gun1–5*), *gun1* encodes a chloroplast-localized pentatricopeptide-repeat protein, which serves as an integrated upstream factor for retrograde signaling [18]. The other four mutants (*gun2–5*) have mutations in genes encoding enzymes of the tetrapyrrole biosynthesis pathway [6,19]. Subsequently, as result of analysis of chlorophyll intermediates of *Chlamydomonas reinhardtii* and Arabidopsis, it was suggested that Mg protoporphyrin IX acts as a potential plastid-derived retrograde signal [20]. However, in more recent reports, a direct correlation between Mg protoporphyrin IX accumulation and retrograde signaling has been doubted [21]. Thus, although the detailed mechanism of retrograde signaling is currently being elucidated, there are still many details that require further investigation.

In this study, we silenced the *CHLI* gene and the previously identified *CHLD* gene [22] in pea plants using virus-induced gene silencing (VIGS). Comprehensive analyses were conducted in these VIGS plants with lower Mg chelatase activity to determine the pigment contents, 5-aminolevulinic acid (ALA) synthesizing capacity, photosynthetic capacity, reactive oxygen species (ROS) metabolism and PhANGs expression as well as the changes in the content of metabolites of primary metabolic pathways. This report includes a first evaluation of primary metabolites in Mg chelatase-inactivated plants and indicates the tight link of metabolic activities in different cellular compartments with changes in chlorophyll biosynthesis. Based on our results we suggest a mechanism of metabolite-mediated interorganellar signaling.

2. Results

2.1. A characteristic yellowish phenotype of the pea VIGS-CHLI and VIGS-CHLD plants

The Pea-Early-Browning-Virus (PEBV)-based VIGS vectors [23] were used for sequence-specific silencing of the pea *CHLI* and *CHLD* genes (Figure S1). Nine to ten days after infiltration (dpi), the upper, non-inoculated leaves from both VIGS-*CHLI* and VIGS-*CHLD* plants altered from green to yellow pigmentation, which is characteristic for reduced chlorophyll content (Figure S2A). The VIGS-induced-yellow-leaf phenotype remained during plant development in the leaves above the infected leaf (Figure S2A). The appearance of the yellow phenotype increased with time and spread from the veins over the entire leaf (Figure S2B). The three types of leaves shown in Fig. 1 represent different stages of virus infection: fully yellow leaves (fy), yellow sectors from mosaic leaves (y/m), green sectors from mosaic leaves (g/m) and fully expanded green leaves (fg). Successful VIGS infection was always associated with the yellow pigmentation of stems (Figure S2A), sepals (Figure S2C), ovaries (Figure S2C) and seed capsula (Figure S2C). Quantitative real-time PCR of the *CHLI* and *CHLD* expression in the yellow leaf tissues (fy and y/m) of VIGS-*CHLI* plants and VIGS-*CHLD* plants revealed reduced *CHLI* and *CHLD* mRNA levels of approximately 90% in comparison to mRNA content in green leaves of similar age of VIGS-*GFP* control plants (Fig. 5A), respectively. Using anti-CHLI and anti-CHLD antibodies, western-blot analysis of the VIGS plants indicates that the CHLI and CHLD contents are below the detection level in the yellow leaf tissues of corresponding VIGS plants (Fig. 5B).

2.2. Reduction in pigment contents, ALA synthesizing capacity and Mg chelatase activity in the yellow leaf tissues of VIGS-CHLI and VIGS-CHLD plants

Further examination of the chimeric phenotype of the VIGS-*CHLI* and VIGS-*CHLD* plants includes the measurements of chlorophyll, carotenoid and anthocyanin contents. In the yellow leaf tissues (fy and y/m) of VIGS-*CHLI* and VIGS-*CHLD* plants, the contents of chlorophyll (Figure S3A), carotenoid (Figure S3C) and anthocyanin (Figure S3D) decreased, while in parallel, the chlorophyll a/b ratios drastically increased (Figure S3B). Even the green tissues (g/m and fg) showed significant changes in the pigment contents in both the *CHLI*- and *CHLD*-silenced plants (Figure S3A, C and D) in comparison to control plants.

Given that we observed strongly decreased chlorophyll contents and highly suppressed *CHLI* and *CHLD* expression in the yellow leaf tissues, we next assayed for Mg chelatase activity and determined significantly decreased enzyme activity in the yellow leaf tissues of VIGS-*CHLI* and VIGS-*CHLD* plants. In comparison to control plants, which were induced by VIGS-*GFP* expression (133.40 ± 4.98 pmol Mg-Deutero min^{-1} mg^{-1} protein), the Mg chelatase activity declined to 5.15 ± 0.15 and 6.16 ± 0.46 pmol Mg-Deutero min^{-1} mg^{-1} protein in the yellow leaf tissues of VIGS-*CHLI* and VIGS-*CHLD* plants, respectively (Table 1). We further asked whether the reduced Mg chelatase activity affects additional steps in the tetrapyrrole biosynthesis pathway and examined the ALA synthesizing capacity and the heme content of the VIGS plants. Remarkably, both the ALA synthesizing capacity and the heme content in the yellow leaf tissues of VIGS-*CHLI* and VIGS-*CHLD* plants were

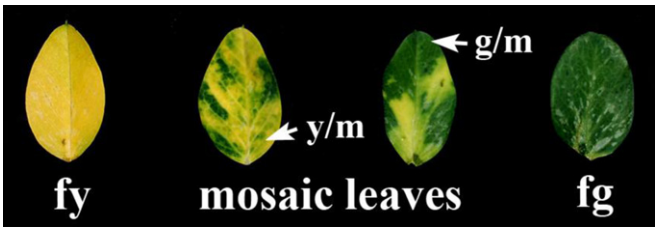

Fig. 1. Representative leaflets of the VIGS-*CHLD* and VIGS-*CHLI* plants. Four types of leaf tissues represent different stages of virus infection: fy, fully yellow leaves; y/m, yellow sectors from mosaic leaves; g/m, green sectors from mosaic leaves; fg, fully expanded green leaves.

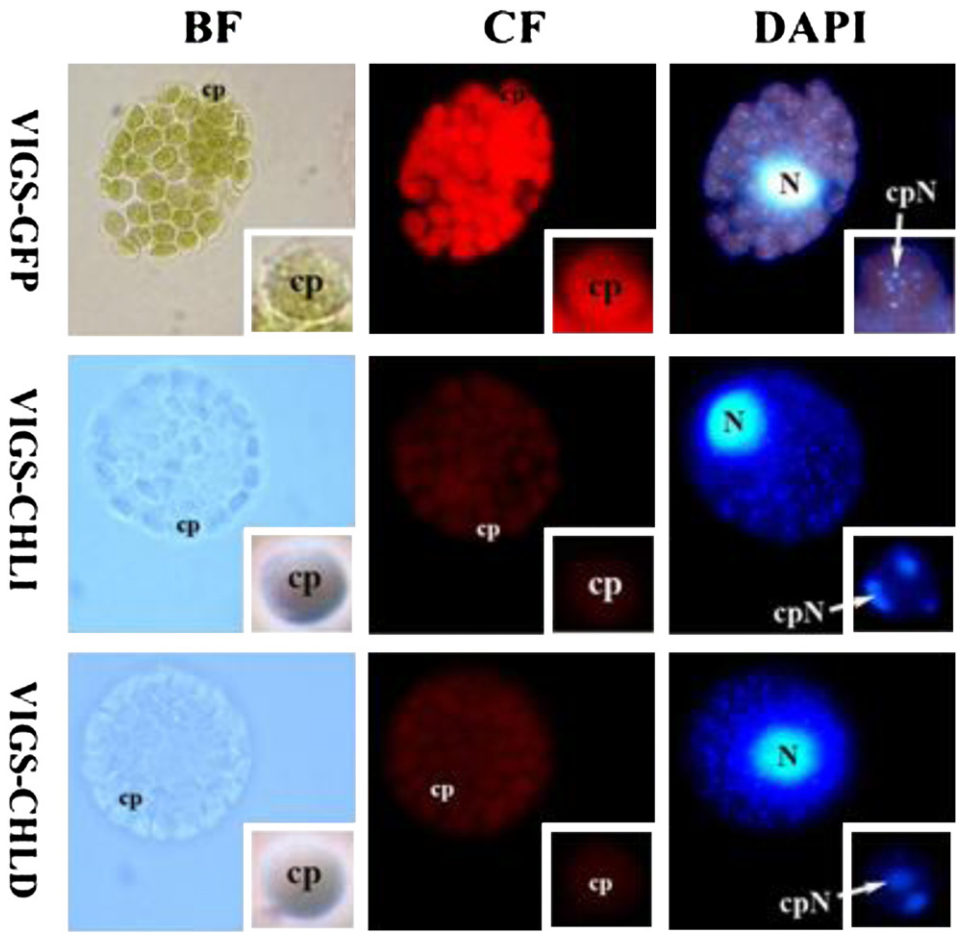

Fig. 2. The nucleoids in the chloroplasts of VIGS plants visualized by DAPI-staining. Protoplasts isolated from the yellow leaf tissues (fy and y/m) of VIGS-*CHLD* and VIGS-*CHLI* plants and the green leaves of VIGS-*GFP* plants were stained by DAPI and visualized using an Olympus BX51 fluorescence microscope, respectively. BF, bright field; CF, chlorophyll autofluorescence; DAPI, DAPI fluorescence excited by UV light; N, nucleus; cp, chloroplast; cpN, chloroplast nucleoid.

significantly down-regulated (Table 1). These results indicate that compromised *CHLI* and *CHLD* expression does not only result in reduced chlorophyll content, but also affects control of ALA and heme biosynthesis.

2.3. Abnormal ultrastructure of chloroplasts and chloroplast nucleoids as well as decreased photosynthesis capacity in the yellow leaf tissues of VIGS-CHLI and VIGS-CHLD plants

Using electron microscopy, we observed in yellow leaf tissues (fy and y/m) of the VIGS-*CHLI* and VIGS-*CHLD* plants abnormal chloroplasts that lack the complete formation of stroma thylakoid membranes and grana stacks as well as the accumulation of starch (Figure S4A). However, in the green tissues (fg and g/m) of these VIGS plants, the chloroplasts are well developed (Figure S4A). The nucleoids of the chloroplasts were visualized using DAPI staining. In the yellow tissues of expanded leaves of the *CHLI*- and *CHLD*-silenced plants the chloroplast nucleoids showed reduced DNA compaction and aggregation in the chloroplasts (cpN in VIGS-*CHLI*/DAPI and VIGS-*CHLD*/DAPI, Fig. 2), while normal nucleoids with highly compacted DNA were detected in the chloroplasts of VIGS-*GFP* control plants (cpN in VIGS-*GFP*/DAPI, Fig. 2).

The chlorophyll fluorescence in the leaves of VIGS plants growing under different light intensities (40 μE, 250 μE and 700 μE) was analyzed in order to determine their photosynthesis capacity. In the yellow tissues, the Fv/Fm ratio decreased with increasing light-intensities (Figure S4B), while in the green tissues, the Fv/Fm ratio did not significantly vary among the VIGS plants (Figure S4B). These results indicate a light-dependent reduction of the maximum quantum efficiency of photosystem II (PSII) in the VIGS-*CHLI* and VIGS-*CHLD* plants as result of reduced Mg chelatase and chlorophyll content.

2.4. ROS accumulation in response to reduced Mg chelatase activity in the yellow leaf tissues of VIGS-CHLI and VIGS-CHLD plants

Because suppressed *CHLI* and *CHLD* expression in the yellow leaf tissues (fy and y/m) of VIGS plants correlates with deformed chloroplasts that contain only an insufficient and disabled thylakoid membrane system (Figure S4A) and low photosynthesis activity (Figure S4C), we further investigated the ROS levels in the yellow tissues (fy and y/m) of VIGS-*CHLI* and VIGS-*CHLD* plants grown under different light conditions (40, 250 and 700 μE). In the full yellow leaves (fy) of the VIGS-*CHLI* and VIGS-*CHLD* plants, O^{2-} and H_2O_2 accumulated in response to increased illumination (Fig. 3A). Inhibition of chlorophyll biosynthesis and, in consequence, low photosynthesis capacities are typical sources for additional ROS generation. We intend to examine the effects of accumulated ROS in the yellow leaf tissues of VIGS-*CHLI* and VIGS-*CHLD* plants on the non-enzymatic antioxidant contents and the activities of antioxidant enzymes. The content of ascorbic acid (Supplementary Table S1) and proline

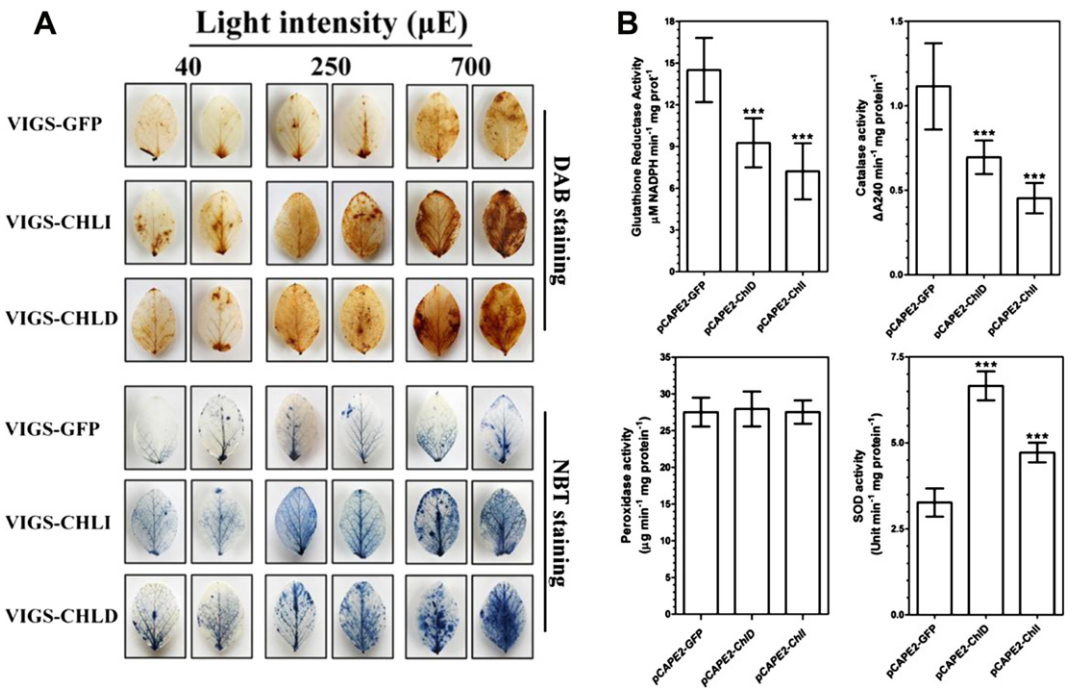

Fig. 3. ROS accumulation and activities of antioxidant enzymes in VIGS plants. The VIGS plants at 10 dpi were grown under different light intensity for 1 week. The newly germinating leaves (the full yellow leaves of VIGS-*CHLD* and VIGS-*CHLI* plants and the green leaves of VIGS-*GFP* plants) were taken for histochemical staining using 3,3′-diaminobenzidine (DAB) and nitroblue tetrazolium (NBT) to show the accumulated H_2O_2 (A, up) and O_2^- (A, down) and for activities of antioxidant enzymes (B), respectively. Data represent the mean ± S.D. of 12 plants from three independent infiltrations. ***$P < 0.0001$ by Student's t test.

(Supplementary Table S1) as well as superoxide dismutase (SOD) activity (Fig. 3B) was up-regulated, while reduced carotenoid (Figure S3D) and anthocyanin (Figure S3C) contents as well as catalase (CAT) and glutathione reductase (GR) activities (Fig. 3B) were determined in the yellow leaf tissues of VIGS-*CHLI* and VIGS-*CHLD* plants compared with the green leaves of VIGS-*GFP* plants. These results suggest that reduced Mg chelatase activity disturbs the balance between ROS production and concurrent ROS detoxification in the yellow leaf tissues of VIGS-*CHLI* and VIGS-*CHLD* plants.

2.5. Modification of metabolites in the yellow leaf tissues of VIGS-CHLI and VIGS-CHLD plants

The ultrastructure of chloroplasts is impaired as a consequence of chlorophyll deficiency in the yellow leaf tissues of *CHLI*- and *CHLD*-silenced plants, which most likely ultimately also affects other pathways of primary metabolism. We next examined the levels of metabolites of major primary pathways expressed in these plants using an established gas-chromatography mass-spectrometry (GC–MS) protocol for metabolic profiling [24]. These studies revealed considerable changes in the levels of a wide range of organic acids, amino acids and sugars (Fig. 4 and Supplementary Table S1). Interestingly, the levels of tricarboxylic acid (TCA) cycle-related metabolites, for example, pyruvate, isocitrate, malate and fumarate, were significantly reduced, while increased levels of 2-oxoglutarate, succinate and γ-amino butyrate (GABA) in the yellow leaf tissues of both the VIGS-*CHLI* and VIGS-*CHLD* plants were observed (Fig. 4). Surprisingly, the levels of the vast majority of amino acids were increased in the yellow leaf tissues of both the VIGS-*CHLI* and VIGS-*CHLD* plants (Fig. 4). Briefly, significant increases in both lines were observed for alanine, β-alanine, arginine, asparagine (240 folds in VIGS-*CHLD* plants and 360 folds in VIGS-*CHLI* plants), cysteine (30 folds in VIGS-*CHLD* plants and 74 folds in VIGS-*CHLI* plants), cystine, isoleucine (3 folds in VIGS-*CHLD* plants and 12 folds in VIGS-*CHLI* plants), lysine, methionine (18 folds in VIGS-*CHLD* plants and 30 folds in VIGS-*CHLI* plants), ornithine (125 folds in VIGS-*CHLD* plants and 175 folds in VIGS-*CHLI* plants), proline, serine, threonine, tryptophan and valine. One unexpected feature of our data set was that the levels of aspartate, glycine and phenylalanine were increased in the yellow leaf tissues of VIGS-*CHLI* plants and reduced in the yellow leaf tissues of VIGS-*CHLD* plants. This result implies a diverse impact of *CHLI*- or *CHLD*-expression on the accumulation of certain metabolites. In addition, the levels of fructose and sucrose were reduced to 25% in both plant lines indicating a decreased photosynthesis capacity. The contents of nitrogen compounds were also changed. Putrescine, one of the polyamines, accumulated to high levels in response to silenced *CHLI* and *CHLD* expression (Fig. 4); a similar response was observed for urea, whereas a significantly reduced spermidine content was demonstrated only in the yellow leaf tissues of VIGS-*CHLD* plants (Fig. 4). Moreover, the level of glycerate, which is a product of photorespiration and the Calvin–Benson cycle, was decreased in the yellow leaf tissues of both the VIGS-*CHLI* and VIGS-*CHLD* plants (Fig. 4). The level of glycerol, which is an intermediate of many metabolic pathways, such as triglyceride biosynthesis and gluconeogenesis, was also decreased in the yellow leaf tissues of VIGS-*CHLD* plants but not in the VIGS-*CHLI* plants (Fig. 4).

2.6. Expression of PhANGs in the yellow leaf tissues of VIGS-CHLI and VIGS-CHLD plants

To further explore the role of Mg chelatase in retrograde signaling, we analyzed the expression of PhANGs in the yellow leaf tissues (fy and y/m) of VIGS plants. The expression of genes involved in photosynthesis (*ribulose-1,5-bisphosphate carboxylase oxygenase small subunit*, *RBCS* and *light-harvesting chlorophyll-binding proteins 3 of photosystem II*, *LHCB3*) and the tetrapyrrole

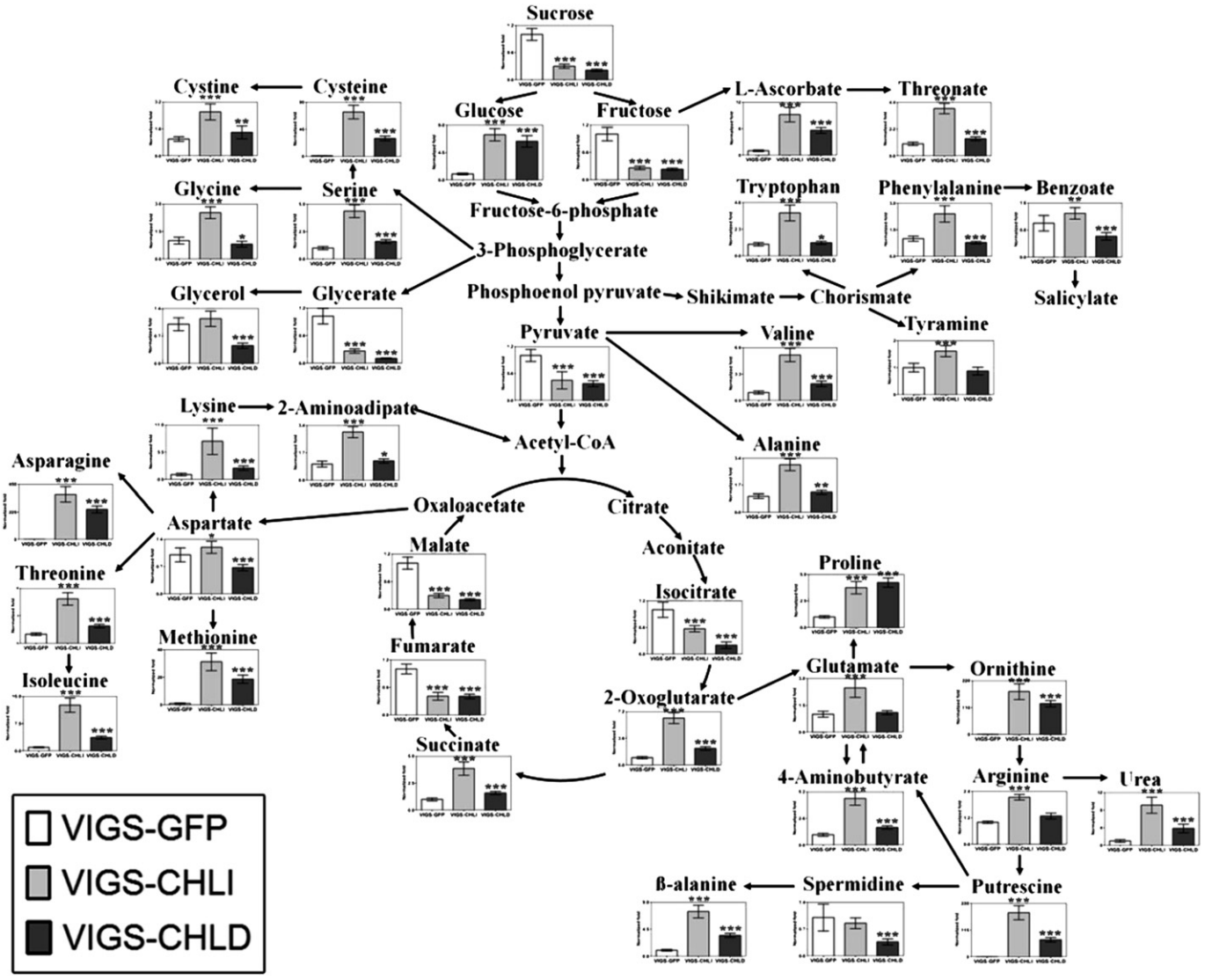

Fig. 4. Metabolite profiling for VIGS-*CHLI* and VIGS-*CHLD* plants. The metabolites in the yellow leaf tissues (fy and y/m) of VIGS-*CHLD* and VIGS-*CHLI* plants were all normalized to the average amount of the green leaves of VIGS-*GFP* plants. The metabolic pathway was described in Ref. [39]. Values presented are means ± SD of 10–12 independent measurements. $^{***}P < 0.0001$, $0.0001 < {}^{**}P < 0.005$, $0.005 < {}^{*}P < 0.05$ by the Student's *t* test.

biosynthesis pathway (*glutamyl-tRNA reductase*, *HEMA1*; *CHLH*; Mg-protoporphyrin IX methyltransferase, *CHLM* and *ferrochelatase I*, *FECH I*) were down-regulated as a consequence of *CHLD* silencing, but, interestingly, not of *CHLI* silencing (Fig. 5A).

The *in vivo* contents of light-harvesting chlorophyll-binding proteins (LHCA1, LHCB1, LHCB5 and LHCB6) were significantly reduced, and CHLH accumulated in the yellow leaf tissues of both the VIGS-*CHLD* and VIGS-*CHLI* plants in comparison to the control samples (Fig. 5B). Non-detectable levels of CHLD and CHLI proteins, reduced GUN4, CHLM, Mg-protoporphyrin IX monomethylester (oxidative) cyclase (CHL27), NADPH-protochlorophyllide oxidoreductase (POR), geranylgeranyl reductase (CHLP) and ribulose-1,5-bisphosphate carboxylase oxygenase small subunit (SSU) contents and increased levels of protoporphyrinogen IX oxidase (PPO), Chlorophyll a oxygenase (CAO) and phytochromobilin synthase (HY2) were observed upon *CHLI* gene silencing, while glutamate 1-semialdehyde aminotransferase (GSAAT), PPO, POR and CAO accumulated and SSU was reduced in response to suppressed *CHLD* expression (Fig. 5B).

3. Discussion

3.1. A deficient chlorophyll content inhibits chloroplast development, resulting in modified chloroplast nucleoids and photosynthesis capacity in the yellow leaf tissues of VIGS-CHLI and VIGS-CHLD plants

As result of VIGS-induced reduction of *CHLI* and *CHLD* expression, the low Mg chelatase activity causes reduced chlorophyll content (Figure S3A), resulting in an undeveloped thylakoid membrane structure during chloroplast biogenesis (Figure S4A). These changes in chlorophyll biosynthesis strongly correlate with reduced contents of light-harvesting chlorophyll-binding proteins (Fig. 5B) that do not sufficiently assemble into photosynthesis antenna complexes in the yellow leaf tissues of VIGS-*CHLI* and VIGS-*CHLD* plants in comparison to VIGS-*GFP* control plants. The less developed chloroplasts are characterized by reduced photosynthesis capacity (F_v/F_m, Figure S4B), and, ultimately, reduced and modified metabolic activities (Supplementary Table S1). These studies indicate that Mg

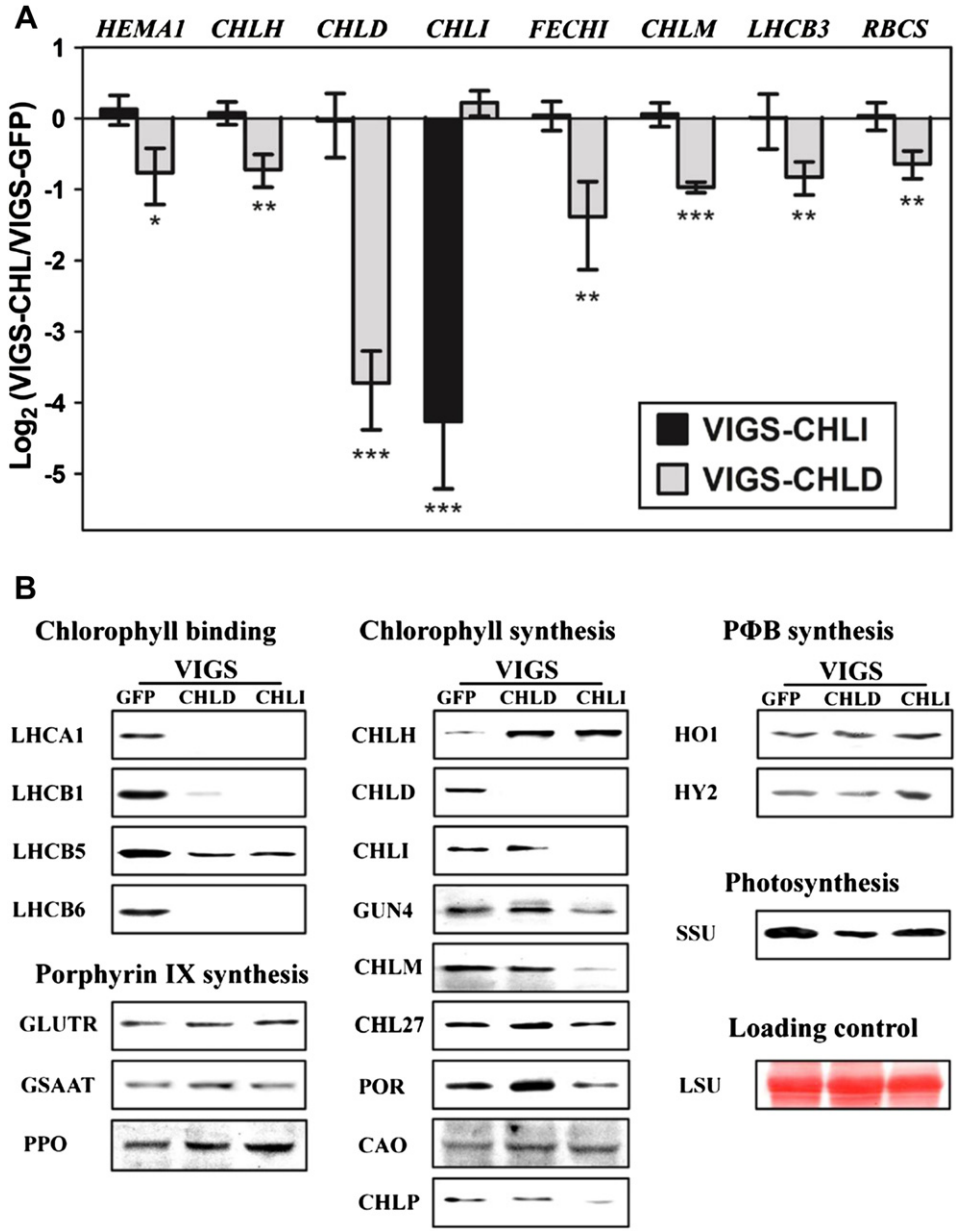

Fig. 5. Determination of the expression of PhANGs in VIGS plants. The expression of PhANGs in the yellow leaf tissues (fy and y/m) of VIGS-*CHLD* and VIGS-*CHLI* plants were analyzed by quantitative real-time PCR normalized to VIGS-GFP plants (Control) using the $2^{-\Delta\Delta Ct}$ method (A) and western blot (B), respectively. The data represent the mean ± S.D. of three independent infiltrations. $^{***}P < 0.0001$, $0.0001 < {}^{**}P < 0.005$ and $0.005 < {}^{*}P < 0.05$ by Student's *t* test. For western blot each lane was loaded with 25 μg of total proteins. LHCA1, light harvesting chlorophyll binding protein 1 of photosystem I; LHCB1, LHCB3, LHCB5, and LHCB6, light harvesting chlorophyll binding protein 1, 3, 5, and 6 of photosystem II, respectively. CHLP, geranylgeranyl reductase; RBCS and SSU, Rubisco small subunit; CHLI, CHLD, and CHLH, the three subunits of Mg chelatase; CHLM, Mg-protoporphyrin IX methyltransferase; CHL27, subunit of Mg-protoporphyrin IX monomethylester (oxidative) cyclase; POR, NADPH-protochlorophyllide oxidoreductase; CAO, chlorophyll a oxygenase; HEMA1 and GLUTR, glutamyl-tRNA reductase; GSAAT, glutamate 1-semialdehyde aminotransferase; PPO, protoporphyrinogen IX oxidase; HO1, heme oxygenase; HY2, phytochromobilin synthase; LSU, Rubisco large subunit.

chelatase has a key regulatory role in chlorophyll synthesis, but ultimately for chloroplast development and photosynthesis.

In higher plants, chloroplasts represent an increased polyploid genetic system with dozens or even hundreds of genome copies that are organized into nucleoids by a set of proteins [25]. In chloroplasts of mature leaves, nucleoids with highly compacted DNA found in subcompartments of plastids are detectable as small blue areas in chloroplasts upon DAPI staining (cpN in VIGS-*GFP*/DAPI, Fig. 2). In the yellow leaf tissues of VIGS-*CHLD* and VIGS-*CHLI*, chloroplasts are characterized by the presence of undeveloped thylakoid membranes and a lack of grana stacks. As result the nucleoids do not show the same organization resulting in chloroplast alteration with reduced DNA compaction and aggregation (cpN in VIGS-*CHLI*/DAPI and VIGS-*CHLD*/DAPI, Fig. 2). To our knowledge, these results are the first experimental data demonstrating a correlation between chlorophyll synthesis and the topology of chloroplast nucleoids, suggesting a regulatory impact of Mg chelatase activity and chlorophyll biosynthesis on chloroplast nucleoids and plastid gene expression.

3.2. *Mg chelatase activity influences interorganellar metabolism in plant cells*

The metabolite profile of these VIGS plants also reflects modified photosynthesis metabolism, including the reduced

Table 1
Heme content, Mg chelatase activity and 5-aminolevulinic acid (ALA) synthesizing capacity in VIGS plants. The green leaves from VIGS-*GFP* plant and the yellow leaf tissues (fully yellow leaves and yellow sectors of mosaic leaves) from VIGS-*CHLI* and VIGS-*CHLD* plants were taken for determination of heme content and enzyme assays as described in the Material and method. $^{***}P < 0.0001$ by Student's *t* test. FW, fresh weight. Data represent the mean ± S.D. of 12 plants from three independent infiltrations.

Parameters of tetrapyrrole biosynthesis	VIGS-*GFP*	VIGS-*CHLI*	VIGS-*CHLD*
Heme (pmol mg^{-1} FW)	25.98 ± 2.16	8.26 ± 1.14***	3.97 ± 0.78***
Mg-chelatase activity (pmol Mg-Deutero min^{-1} mg^{-1} protein)	133.40 ± 4.98	5.15 ± 0.15***	6.16 ± 0.46***
ALA synthesizing capacity (nmol ALA h^{-1} g^{-1} FW)	194.00 ± 22.21	78.25 ± 11.27***	95.57 ± 8.03***

Calvin–Benson cycle activities and decreased starch, sucrose, fructose and pyruvate contents in the yellow leaf tissues of both VIGS-*CHLD* and VIGS-*CHLI* plants compared with the green leaves of VIGS-*GFP* control plants (Fig. 4). These alterations also led to changes in secondary metabolites, such as anthocyanins (Figure S3C), ascorbic acid, putrescine, spermidine and urea (Supplementary Table S1). Most of the free amino acids were significantly increased in the yellow leaf tissues of both the VIGS-*CHLI* and VIGS-*CHLD* plants (Fig. 4), which suggests that protein degradation was elevated in these plants. The levels of the branched chain amino acids isoleucine and valine were increased in these VIGS plants. Recent evidence has demonstrated that branched chain amino acids feed electrons into the mitochondrial electron transport chain, particularly under carbohydrate-scarce conditions [26], as observed here. In the yellow leaf tissues of VIGS-*CHLI* and VIGS-*CHLD* plants, the reduced photosynthesis activity correlates with compromised accumulation of sucrose (Fig. 4). Sucrose starvation activates protein degradation and results in the accumulation of free amino acids to supply respiratory substrates to the TCA cycle. Therefore, the content of several organic acids that serve as intermediates of the TCA cycle, was significantly changed in the yellow leaf tissues of VIGS-*CHLI* and VIGS-*CHLD* plants (Fig. 4 and Supplementary Table S1). Alternatively, the change in these metabolites can be, at least partially, explained by the operation of different light flux modes. A recent study of the light-exposed rice *oschlh* mutant revealed low content of ATP and cytosolic NADH, which is indicative for an inhibition of the mitochondrial metabolism [27]. Our metabolomics data are consistent with previous reports suggesting a tight coordination of metabolic pathways in both organelles. It is reasonable to conclude that the relative activities of photosynthesis and respiratory pathways for energy production are carefully regulated within plant cells in balance to the synthesis of photosynthetic pigments. Taken together, as Mg chelatase activity also balances ALA synthesis in response to chlorophyll biosynthesis, and as plant metabolism is tremendously affected in plants with modified Mg chelatase activity, it is suggested that Mg chelatase serves as an important regulator of not only tetrapyrrole biosynthesis, but also of the primary interorganellar metabolic pathways in plant cells.

3.3. Altered activities of Mg chelatase results in the accumulation of ROS

Accumulated tetrapyrrole intermediates in chloroplasts are phototoxic and generate ROS upon light exposure [28]. In transformed tobacco plants with impaired expression of coproporphyrinogen oxidase, plastidic ferrochelatase and Mg protoporphyrin monomethylester (MgProtoME) cyclase, the over-accumulation of photooxidative protoporphyrin, Mg protoporphyrin or MgProtoME results in ROS accumulation, which can generate the signals to activate expression of antioxidant genes and elevate the antioxidant contents and activity of the antioxidant enzymes. But, the elevated capacity of antioxidant defense system can only scavenge part of the over-accumulated ROS that causes a light intensity-dependent formation of necrotic leaf lesions [29]. However, transgenic plants with reduced contents of Mg chelatase and Mg protoporphyrin methyltransferase accumulate no or only low amounts of protoporphyrin and Mg protoporphyrin [30,31]. These previous results indicate that in response to impaired gene expression in tetrapyrrole biosynthesis, regulatory feedback mechanisms prevent the accumulation of non-metabolized tetrapyrrole intermediates only at few enzymatic steps.

In the present study, the yellowish leaves of the VIGS-*CHLI* and VIGS-*CHLD* plants did not show a necrotic phenotype when exposed to different light intensities (Figure S4B). This observation correlates with simultaneous reduction in Mg chelatase activity and ALA biosynthesis rate (Table 1) and can be explained with feedback regulation at the step of Mg chelatase on ALA synthesis that facilitates a reduction in the flux of metabolites of the tetrapyrrole biosynthetic pathway and an avoidance of accumulating tetrapyrrole intermediates. However, this metabolic control does apparently not prevent the accumulation of ROS (Fig. 3A). The balance between ROS production and concurrent ROS detoxification seems to be disturbed in the yellow leaf tissues of VIGS-*CHLI* and VIGS-*CHLD* plants. Thus, it is proposed that inactivation of enzymatic steps of the Mg branch, including Mg chelatase and the cyclase, results in the accumulation of ROS through different mechanisms. Regulated Mg chelatase activity is required to maintain ROS homeostasis for an appropriate redox state in chloroplasts.

3.4. CHLD feedback regulates the transcription of PhANGs

The *Arabidopsis CHLD* mutant (*CHLD KO*) was presented to show the *gun* phenotype. Consistent with previous reports showing that the redox signals generated by ROS can be regarded as retrograde signals that affect the expression of PhANGs [16], we found that ROS accumulates and PhANG expression is modified in response to silenced *CHLD* expression (Figs. 3A and 5A). Thus, we hypothesize that modulated *CHLD* expression affects PhANGs transcription through ROS mediated redox-signaling. However, although ROS accumulates in *CHLI*-silencing plants (Fig. 3A), the transcription of PhANGs is not affected (Fig. 5A). The previous review reported that the Arabidopsis *CHLI1* mutants did not show the *gun* phenotype [16]. But a *chli1*/*chli2* double mutant shows a *gun* phenotype [32]. Taken together, these results imply that both CHLI1 and CHLI2 mutually are involved in retrograde signaling. We speculate that CHLD is more directly involved in emission of retrograde signals derived from tetrapyrrole biosynthesis than CHLI.

3.5. Silenced CHLD and CHLI expression causes in vivo changes in proteins involved in the tetrapyrrole biosynthesis pathway

The tetrapyrrole biosynthesis pathway plays an essential role in plant development and is tightly regulated. Our western blot data (Fig. 5B) showed that several of examined proteins that are involved in tetrapyrrole biosynthesis are characterized by modulated contents in the yellow leaf tissues of VIGS-*CHLI* and VIGS-*CHLD* plants. In addition to the *CHLD*-mediated transcriptional regulation of PhANGs, we hypothesized that Mg chelatase regulates the tetrapyrrole biosynthesis pathway at the transcriptional and post-transcriptional levels. In the yellow leaf tissues of VIGS-*CHLI* plants, the level of CHLD was significantly reduced, consistent with a previous finding that CHLI stabilizes CHLD *in vivo* and acts as a chaperone [15]. Surprisingly, CHLH accumulated

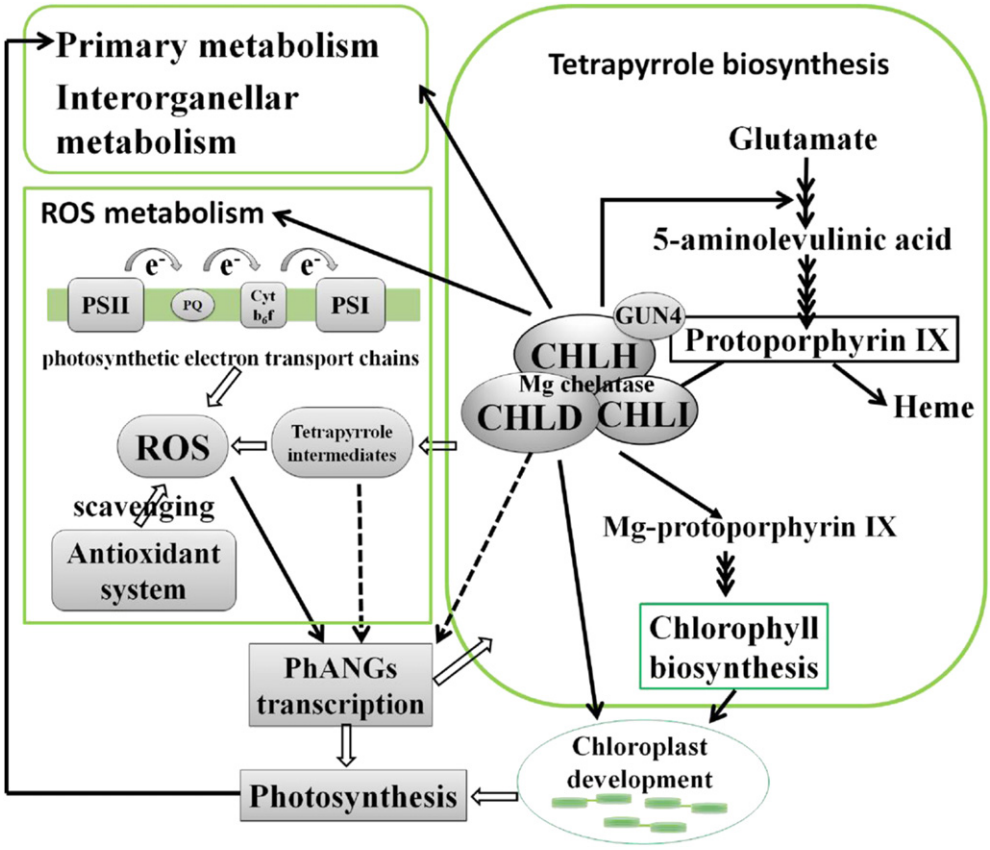

Fig. 6. A proposed regulatory network of Mg chelatase. CHLD, CHLH and CHLI, Mg chelatase subunits CHLD, CHLH and CHLI; Cytb_6f, cytochrome b_6f complex; PhANGs, photosynthesis-associated nuclear genes; PQ, plastoquinone; PSI and PSII, photosystem I and II; ROS, reactive oxygen species. See text for this model in detail.

despite unchanged and reduced levels of the corresponding mRNA in the yellow leaf tissues of VIGS-*CHLI* plants and VIGS-*CHLD* plants, respectively. Similar results of increased CHLH content have also been reported for the *Arabidopsis CHLM* mutant [33] and for thioredoxin F/thioredoxin M double-silenced plants [14]. These findings suggest that CHLH stability is under a complex regulation including protein degradation and signaling [6,34]. It is proposed that reduced Mg chelation reduces the turnover of CHLH resulting in an elevated protein content.

4. Conclusion

In summary, we establish a proposed model to reveal the regulatory role of Mg chelatase in plant cell (Fig. 6). Once the Mg chelatase is inactive in plants, the chlorophyll biosynthesis will stop to feedback regulates tetrapyrrole biosynthesis and result in distorted chloroplast development with altered topological structures of chloroplast nucleoids. During light exposure, modification of the photosynthetic electron transport chains in thylakoid membranes and the tetrapyrrole intermediates can generate ROS, which are normally scavenged by antioxidants. An inactive Mg chelatase causes an imbalance of the ROS metabolism. Then accumulating ROS contribute to plastid-derived retrograde signaling coordinating the PhANG-transcription. In addition, Mg chelatase is also important for modulation of the mitochondrial metabolism (Fig. 6). These interactions of Mg chelatase and tetrapyrrole biosynthesis with the metabolic activities in both organelles are seemingly essential for the proper maintenance of intracellular redox gradients to allow for considerable rates of photorespiration and efficient photosynthesis.

5. Materials and methods

5.1. VIGS assay

To construct pCAPE2-CHLD and pCAPE2-CHLI, a 471-bp fragment of pea CHLD cDNA and a 470-bp fragment of pea CHLI cDNA were generated using RT-PCR and sequence-specific primers (Supplementary Table S2) and were subsequently inserted into the pCAPE2 vector [23] using NcoI and EcoRI sites, respectively. The pCAPE1 and pCAPE2 derivatives were inoculated into *Pisum sativum* (cv. Torsdag; JI992) plants through *Agrobacterium*-infiltration, as described in Ref. [23]. The non-infected plants and the VIGS plants were grown in growth chambers (20 °C, 65% relative humidity, 250 μmol m^{-2} s^{-1}, 14/10 h light/dark photoperiod).

5.2. Determination of heme and pigment contents

Heme was extracted from Frozen leaf material and determined by HPLC analysis (Agilent 1200 Infinity series) as described [35]. The chlorophyll and carotenoids were extracted with 100% acetone, and their concentrations were determined spectrophotometrically according to the Lambert–Beer law. Anthocyanins were extracted by homogenizing leaves (approximate 0.1 g) in a precooled mortar with 1 ml of acidified (1% HCl) methanol and maintained at 4 °C overnight in the dark. Particulates were removed by centrifugation at 16,000× *g* for 20 min and the supernatant was taken to analyze spectrophotometrically. Anthocyanins were calculated by using $Abs_{530}-0.25Abs_{657}$. Spectrophotometric analysis was performed using a Beckman DU-730 spectrophotometer.

5.3. Determination of ALA synthesizing capacity and enzyme activities

The ALA synthesizing capacity was determined as previously described [14]. The ATPase activity was measured according to reference [13]. To measure the Mg chelatase activity, intact chloroplasts were isolated from less expanded leaflets of the VIGS plants. The Mg chelatase activity was determined using a stopped fluorometric assay, as described in Ref. [36]. The activities of four antioxidant enzymes, catalase (CAT, EC 1.11.1.6), peroxidase (POD, EC 1.11.1.7), superoxide dismutase (SOD, EC 1.15.1.1) and glutathione reductase (GR, EC 1.8.1.7), were spectrophotometrically measured using detection kits (Nanjing Jiancheng Bioengineering Institute, China) and described previously.

5.4. Microscopy analysis

To observe the ultrastructure of the chloroplasts, the leaflets from the VIGS plants were cut into 0.5- to 1.0-mm pieces, vacuum-infiltrated and pre-fixed in a solution of 2.5% glutaraldehyde adjusted to pH 7.4 with 0.1 M phosphate buffer, fixed in 2% OsO_4 in the same buffer, and then dehydrated and embedded in epoxy resin. Ultra-thin sections obtained using a Leica UC6 ultramicrotome were stained with uranyl acetate and subsequently with lead citrate. The observations and recording of images were performed using a Hitachi H-7650 transmission electron microscope at 80 kV and a Gatan 832 CCD camera. Visualization of the chloroplast nucleoids was performed according to [25] using an Olympus BX51 fluorescence microscope equipped with UV (340–380 nm) and green (558–582 nm) filters.

5.5. Measurement of chlorophyll fluorescence and ROS

Chlorophyll fluorescence imaging was performed using a chlorophyll imaging system (Closed FC 700-C, Photon Systems Instruments). The chlorophyll fluorescence images and photosynthesis parameters were processed using FluorCam v 5.0 software (Photon Systems Instruments). Before each measurement, the plants were dark-adapted for 20 or 60 min. The in situ accumulation of O^{2-} and H_2O_2 was examined based on histochemical staining with nitroblue tetrazolium (NBT) and with 3,3′-diaminobenzidine (DAB) as described previously [32].

5.6. GC–MS-based metabolite profiling in VIGS plants

Approximately 100 mg of green leaves from the VIGS-*GFP* plants and 100 mg of yellow leaf tissues from the VIGS-*CHLI* and VIGS-*CHLD* plants were ground in liquid nitrogen. The plant metabolites were extracted and analyzed as previously described [24]. The metabolites were identified through comparisons with database entries of authentic standards [37]. The metabolite profiling data are reported in accordance with recent recommendations [38] (*see* Supplementary Table S3).

5.7. Quantitative real-time PCR and western blot analysis

The top and premature leaves of VIGS plants at 21 days after infiltration (dpi) were harvested after the first hour of light exposure and the daily transition from dark to light. Total RNA and proteins were extracted from these leaves described previously [14]. Quantitative real-time PCR and western blot were performed as described previously [14]. The transcript levels were normalized to the transcript level of pea GAPN (Accession No.: U34988). The primers used in the quantitative real-time PCR amplifications are described in Supplementary Table S2. The antibody data are shown in Supplementary Table S4.

Acknowledgments

We are grateful to Dr. Ida Elisabeth Johansen for the gift of the VIGS vectors; Prof. Da Luo for the gift of the pea seeds as well as the VIGS vectors; Dr. Shuaixiang Zhou for the gift of the plasmids pET28a-OsCHLD, pET28a-OsCHLH and pET28a-OsGUN4 and Prof. Ayumi Tanaka for the gift of the anti-CAO antibody. We thank Dr. Lars Dietzel for technical assistance with chlorophyll fluorescence analysis; Dr. Boris Hedtke for the technical guide with laser confocal microscopy and An Yu for the help of quantitative real-time PCR. We also thank Jianbo Cao from the public laboratory of electron microscopy in Huazhong Agricultural University for technical assistance with microscopy analysis. This work was supported by National Natural Science Foundation of China (Grant No. 30971748), the Chinese 111 Project (Grant No. B07041) and a FOR 804 project of the Deutsche Forschungsgemeinschaft (BG).

Appendix A. Supplementary data

Supplementary data related to this article can be found at http://dx.doi.org/10.1016/j.plaphy.2013.01.006.

References

[1] T. Masuda, Recent overview of the Mg branch of the tetrapyrrole biosynthesis leading to chlorophylls, Photosynth. Res. 96 (2008) 121–143.
[2] L.C. Gibson, R.D. Willows, C.G. Kannangara, D. von Wettstein, C.N. Hunter, Magnesium-protoporphyrin chelatase of *Rhodobacter sphaeroides*: reconstitution of activity by combining the products of the *bchH*, *-I*, and *-D* genes expressed in *Escherichia coli*, Proc. Natl. Acad. Sci. U. S. A. 92 (1995) 1941–1944.
[3] R.D. Willows, S.I. Beale, Heterologous expression of the *Rhodobacter capsulatus BchI*, *-D*, and *-H* genes that encode magnesium chelatase subunits and characterization of the reconstituted enzyme, J. Biol. Chem. 273 (1998) 34206–34213.
[4] P.E. Jensen, R.D. Willows, B.L. Petersen, U.C. Vothknecht, B.M. Stummann, C.G. Kannangara, D. von Wettstein, K.W. Henningsen, Structural genes for Mg-chelatase subunits in barley: *Xantha-f*, *-g* and *-h*, Mol. Genet. Genomics 250 (1996) 383–394.
[5] B.L. Petersen, M.G. Møller, P.E. Jensen, K.W. Henningsen, Identification of the *Xan-g* gene and expression of the mg-chelatase encoding genes *Xan-f*, *-g* and *-h* in mutant and wild type barley (*Hordeum vulgare* L.), Hereditas 131 (1999) 165–170.
[6] N. Mochizuki, J. Brusslan, R. Larkin, A. Nagatani, J. Chory, Arabidopsis genomes uncoupled 5 (GUN5) mutant reveals the involvement of Mg-chelatase H subunit in plastid-to-nucleus signal transduction, Proc. Natl. Acad. Sci. U. S .A. 98 (2001) 2053.
[7] C.J. Walker, J.D. Weinstein, The magnesium-insertion step of chlorophyll biosynthesis is a two-stage reaction, Biochem. J. 299 (Pt 1) (1994) 277–284.
[8] J. Lundqvist, H. Elmlund, R.P. Wulff, L. Berglund, D. Elmlund, C. Emanuelsson, H. Hebert, R.D. Willows, M. Hansson, M. Lindahl, S. Al-Karadaghi, ATP-induced conformational dynamics in the AAA^{+} motor unit of magnesium chelatase, Structure 18 (2010) 354–365.
[9] M.N. Fodje, A. Hansson, M. Hansson, J.G. Olsen, S. Gough, R.D. Willows, S. Al-Karadaghi, Interplay between an AAA module and an integrin I domain may regulate the function of magnesium chelatase, J. Mol. Biol. 311 (2001) 111–122.
[10] N.D. Adhikari, J.E. Froehlich, D.D. Strand, S.M. Buck, D.M. Kramer, R.M. Larkin, GUN4-porphyrin complexes bind the ChlH/GUN5 subunit of Mg-Chelatase and promote chlorophyll biosynthesis in Arabidopsis, Plant Cell 23 (2011) 1449–1467.
[11] S. Zhou, A. Sawicki, R.D. Willows, M. Luo, C-terminal residues of *Oryza sativa* GUN4 are required for the activation of the ChlH subunit of magnesium chelatase in chlorophyll synthesis, FEBS Lett. 586 (2012) 205–210.
[12] L.C. Gibson, P.E. Jensen, C.N. Hunter, Magnesium chelatase from *Rhodobacter sphaeroides*: initial characterization of the enzyme using purified subunits and evidence for a *BchI–BchD* complex, Biochem. J. 337 (1999) 243–251.
[13] A. Ikegami, N. Yoshimura, K. Motohashi, S. Takahashi, P.G.N. Romano, T. Hisabori, K.-I. Takamiya, T. Masuda, The CHLI1 subunit of *Arabidopsis thaliana* magnesium chelatase is a target protein of the chloroplast thioredoxin, J. Biol. Chem. 282 (2007) 19282–19291.
[14] T. Luo, T. Fan, Y. Liu, M. Rothbart, J. Yu, S. Zhou, B. Grimm, M. Luo, Thioredoxin redox regulates ATPase activity of magnesium chelatase CHLI subunit and

modulates redox-mediated signaling in tetrapyrrole biosynthesis and homeostasis of reactive oxygen species in pea plants, Plant Physiol. 159 (2012) 118–130.
[15] V. Lake, U. Olsson, R.D. Willows, M. Hansson, ATPase activity of magnesium chelatase subunit I is required to maintain subunit D in vivo, Eur. J. Biochem. 271 (2004) 2182–2188.
[16] A. Nott, H.-S. Jung, S. Koussevitzky, J. Chory, Plastid-to-nucleus retrograde signaling, Annu. Rev. Plant Biol. 57 (2006) 739–759.
[17] R.E. Susek, F.M. Ausubel, J. Chory, Signal transduction mutants of Arabidopsis uncouple nuclear *CAB* and *RBCS* gene expression from chloroplast development, Cell 74 (1993) 787–799.
[18] S. Koussevitzky, A. Nott, T.C. Mockler, F. Hong, G. Sachetto-Martins, M. Surpin, J. Lim, R. Mittler, J. Chory, Signals from chloroplasts converge to regulate nuclear gene expression, Science 316 (2007) 715–719.
[19] R.M. Larkin, J.M. Alonso, J.R. Ecker, J. Chory, GUN4, a regulator of chlorophyll synthesis and intracellular signaling, Science 299 (2003) 902–906.
[20] A. Strand, T. Asami, J. Alonso, J.R. Ecker, J. Chory, Chloroplast to nucleus communication triggered by accumulation of Mg-protoporphyrin IX, Nature 421 (2003) 79–83.
[21] N. Mochizuki, R. Tanaka, A. Tanaka, T. Masuda, A. Nagatani, The steady-state level of Mg-protoporphyrin IX is not a determinant of plastid-to-nucleus signaling in Arabidopsis, Proc. Natl. Acad. Sci. U. S. A. 105 (2008) 15184–15189.
[22] M. Luo, J.D. Weinstein, C.J. Walker, Magnesium chelatase subunit D from pea: characterization of the cDNA, heterologous expression of an enzymatically active protein and immunoassay of the native protein, Plant Mol. Biol. 41 (1999) 721–731.
[23] G.D. Constantin, B.N. Krath, S.A. MacFarlane, M. Nicolaisen, I. Elisabeth Johansen, O.S. Lund, Virus-induced gene silencing as a tool for functional genomics in a legume species, Plant J. 40 (2004) 622–631.
[24] J. Lisec, N. Schauer, J. Kopka, L. Willmitzer, A.R. Fernie, Gas chromatography mass spectrometry-based metabolite profiling in plants, Nat. Protoc. 1 (2006) 387–396.
[25] C.L. Chi-Ham, M.A. Keaton, G.C. Cannon, S. Heinhorst, The DNA-compacting protein DCP68 from soybean chloroplasts is ferredoxin: sulfite reductase and co-localizes with the organellar nucleoid, Plant Mol. Biol. 49 (2002) 621–630.
[26] W.L. Araújo, T. Tohge, K. Ishizaki, C.J. Leaver, A.R. Fernie, Protein degradation an alternative respiratory substrate for stressed plants, Trends Plant Sci. 16 (2011) 489–498.
[27] C.-H. Goh, K. Satoh, S. Kikuchi, S.-C. Kim, S.-M. Ko, H.-G. Kang, J.-S. Jeon, C. Kim, Y.-I. Park, Mitochondrial activity in illuminated leaves of chlorophyll-deficient mutant rice (*OsCHLH*) seedlings, Plant Biotechnol. Rep. 4 (2010) 281–291.
[28] A. Stenbaek, P.E. Jensen, Redox regulation of chlorophyll biosynthesis, Phytochemistry 71 (2010) 853–859.
[29] E. Peter, M. Rothbart, M.-L. Oelze, N. Shalygo, K.-J. Dietz, B. Grimm, Mg protoporphyrin monomethylester cyclase deficiency and effects on tetrapyrrole metabolism in different light conditions, Plant Cell Physiol. 51 (2010) 1229–1241.
[30] J. Papenbrock, E. Pfündel, H.-P. Mock, B. Grimm, Decreased and increased expression of the subunit CHL I diminishes Mg chelatase activity and reduces chlorophyll synthesis in transgenic tobacco plants, Plant J. 22 (2000) 155–164.
[31] A.E. Alawady, B. Grimm, Tobacco Mg protoporphyrin IX methyltransferase is involved in inverse activation of Mg porphyrin and protoheme synthesis, Plant J. 41 (2005) 282–290.
[32] Y.-S. Huang, H.-M. Li, Arabidopsis CHLI2 can substitute for CHLI1, Plant Physiol. 150 (2009) 636–645.
[33] D. Pontier, C. Albrieux, J. Joyard, T. Lagrange, M.A. Block, Knock-out of the magnesium protoporphyrin IX methyltransferase gene in Arabidopsis, J. Biol. Chem. 282 (2007) 2297–2304.
[34] Y. Shang, L. Yan, Z.-Q. Liu, Z. Cao, C. Mei, Q. Xin, F.-Q. Wu, X.-F. Wang, S.-Y. Du, T. Jiang, X.-F. Zhang, R. Zhao, H.-L. Sun, R. Liu, Y.-T. Yu, D.-P. Zhang, The Mg-chelatase H subunit of Arabidopsis antagonizes a group of WRKY transcription repressors to relieve ABA-responsive genes of inhibition, Plant Cell 22 (2010) 1909–1935.
[35] O. Czarnecki, E. Peter, B. Grimm, Methods for analysis of photosynthetic pigments and steady-state levels of intermediates of tetrapyrrole biosynthesis, Methods Mol. Biol. 775 (2011) 357–385.
[36] R. Guo, M. Luo, J.D. Weinstein, Magnesium-chelatase from developing pea leaves, Plant Physiol. 116 (1998) 605–615.
[37] N. Schauer, D. Steinhauser, S. Strelkov, D. Schomburg, G. Allison, T. Moritz, K. Lundgren, U. Roessner-Tunali, M.G. Forbes, L. Willmitzer, A.R. Fernie, J. Kopka, GC–MS libraries for the rapid identification of metabolites in complex biological samples, FEBS Lett. 579 (2005) 1332–1337.
[38] A.R. Fernie, A. Aharoni, L. Willmitzer, M. Stitt, T. Tohge, J. Kopka, A.J. Carroll, K. Saito, P.D. Fraser, V. DeLuca, Recommendations for reporting metabolite data, Plant Cell 23 (2011) 2477–2482.
[39] N. Schauer, A.R. Fernie, Plant metabolomics: towards biological function and mechanism, Trends Plant Sci. 11 (2006) 508–516.